Multi-level computational modeling and quantitative analysis of bone remodeling

Nicola Paoletti, Pietro Liò, Emanuela Merelli and Marco Viceconti

Abstract—Our work focuses on bone remodeling with a multiscale breadth that ranges from modeling intracellular and intercellular RANK/RANKL signaling to tissue dynamics, by developing a multi-level modeling framework. Several important findings provide clear evidences of the multiscale properties of bone formation and of the links between RANK/RANKL and bone density in healthy and disease conditions. Recent studies indicate that the circulating levels of OPG and RANKL are inversely related to bone turnover and bone mineral density and contribute to the development of osteoporosis in post-menopausal women, and thalassemic patients. We make use of a spatial process algebra, the Shape Calculus, to control stochastic cell agents that are continuously remodeling the bone. We found that our description is effective for such a multiscale, multi-level process and that RANKL signaling small dynamic concentration defects are greatly amplified by the continuous alternation of absorption and formation resulting in large structural bone defects. This work contributes to the computational modeling of complex systems with a multi-level approach connecting formal languages and agent-based simulation tools.

Index Terms—Osteoporosis, multi-level, Shape Calculus, bone remodeling, multiscale, RANK/RANKL, agent-based simulation

1 Introduction

Osteoporosis is a skeletal disease characterized by low bone density and structural fragility, which consequently leads to frequent micro-damages and spontaneous fractures. This disease affects primarily middle-aged women and elderly people and at present its social and economic impact is dramatically increasing, so much that the World Health Organization considers it to be the second-leading health-care problem. Osteoporosis and many other bone pathologies are attributable to disorders in the mechanism of bone remodeling (BR), the process by which aged bone is continuously renewed in a balanced alternation of bone resorption and formation. Bone remodeling plays an essential role in repairing micro-damages, in maintaining mineral homeostasis and in the structural adaptation of bone in response to mechanical stress. In healthy conditions the balance between the resorption phase, performed by cells called *osteoclasts*, and the formation phase, performed by *osteoblasts*, ensures the "good quality" of the bone. On the contrary, several diseases can be ascribed to the imbalance between resorption and formation: osteoporosis is an example of negative remodeling that is, when the resorption process prevails on the formation one.

An important factor affecting bone metabolism is *RANK/RANKL/OPG signaling*, depicted in Fig. 1. RANK is a protein expressed by *osteoclasts*; RANK is a receptor for RANKL, a protein produced by *osteoblasts*. RANK/RANKL signaling triggers osteoclast differentiation, proliferation and activation, thus it prominently affects the resorption phase during bone remodeling. Osteoprotegerin (OPG) is a decoy receptor for RANKL. It is expressed by mature osteoblasts and it binds with RANKL, thus inhibiting the production of osteoclasts. Several important findings provide clear evidence of the multiscale properties of bone formation and of the links between RANK/RANKL and bone density in healthy and disease conditions. However, there is a lack of knowledge of the genetic and environmental factors responsible for age and gender specific differences in bone fragility and fracture rates. Recent studies indicate that the circulating levels of RANKL are inversely related to bone turnover and *Bone Mineral Density (BMD)* and contribute to the development of osteoporosis in post-menopausal women [1], and of thalassemia-induced osteoporosis [2].

This paper focuses on modeling the multiscale dynamics of bone remodeling, showing that small changes in RANKL concentration at molecular level can lead to significant disruptions at tissue level, and to important pathologies like osteoporosis. In particular we are interested in assessing the emergence of osteoporosis in older patients, that are typically characterized by a reduced cellular activity, in terms of lower bone formation and resorption rates; lower growth rates; and higher death rates. Two different classes of patients are compared:

- *N. Paoletti and E. Merelli are with the School of Science and Technology, University of Camerino, Italy.*
  Email: `name.surname@unicam.it`
- *P. Liò is with the Computer Laboratory, University of Cambridge, United Kingdom.*
  Email: `pl219@cam.ac.uk`
- *M. Viceconti is with the Department of Mechanical Engineering, University of Sheffield, United Kingdom.*
  Email: `m.viceconti@sheffield.ac.uk`

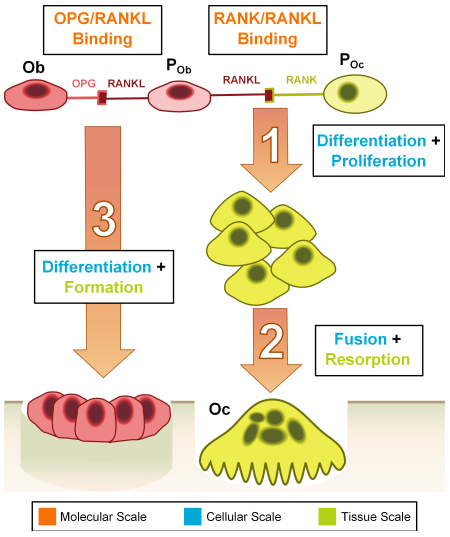

Fig. 1. RANK/RANKL/OPG pathway in bone remodeling involving osteoclasts (Oc), osteoblasts (Ob), and their precursors (P_{Oc} and P_{Ob}, resp.). RANK/RANKL signaling triggers osteoclasts' differentiation and proliferation. RANKL/OPG inhibits osteoclasts' recruitment and induces osteoblasts' maturation. The process spans different scales: molecular, cellular and tissue.

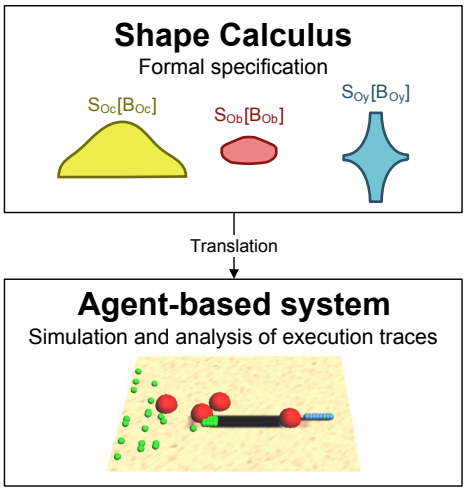

Fig. 2. Multilevel modeling framework. The Shape Calculus algebraic specification is translated into an executable agent-based model. In the upper box, bone cells are drawn as Shape Calculus processes. The lower box shows a snapshot of the simulated system.

- *healthy patients*, with regular RANKL levels and cellular activity, and
- *osteoporotic patients*, with an overproduction of RANKL and a reduced cellular activity.

From a methodological point of view, we define a multi-level modeling framework (depicted in Fig. 2) combining a high-level process-algebraic specification, and a low-level stochastic agent-based simulation [3], [4]. The specification language is the Shape Calculus, a spatial process algebra for describing biological systems [5], [6] and more generally, suitable for systems characterized by a strong interplay between physical and computational features, also known as *cyberphysical systems*. We show how the Shape Calculus allows us to express in a uniform and straightforward way the multiscale nature of bone remodeling involving the molecular, the cellular and the tissue level. While we aim to keep the specification language as generic as possible, the agent-based model is refined with additional features such as *stochasticity*, enriching agents' actions with stochastic rates modeling the propensity of the action; and *perception*, that is the capability to communicate at distance and sense the neighborhood. The agent-based level provides an executable implementation of the process-algebraic one, and it can be formally derived from the specification by applying a set of translation functions. This level enables the analysis of qualitative and quantitative results from the simulation of the model such as tabular data, plots, and 3D views of the agents and their environment.

Our work gives new biological insights into the bone remodeling process, regarded as a multiscale complex biological system [7], and in particular into the link between imbalances in the molecular concentration of RANKL and the occurrence of defective bone pathologies. We show that the combination of higher RANKL levels with a lower cellular activity leads to negative remodeling phenomena and after several remodeling cycles, to severe bone loss, microstructural degradation and osteoporosis. In addition, the proposed computational framework couples a formal specification level with an agent-based simulation level. The former provides a better expressiveness of the BR process, from the intercellular signaling to tissue dynamics. The latter provides a simulation environment for Shape Calculus specifications and a diagnostic tool for comparing different classes of patients, and for analyzing the bone mass and structure; the individual evolution of bone cells; and the concentration levels of RANKL. We believe that the proposed framework could help in understanding the multiscale dynamics of bone remodeling and possibly contribute to the application of predictive computational models as diagnostic tools in personalized medicine and in everyday clinical practice.

The paper is organized as follows. Section 2 introduces the process of bone remodeling and how it is related to bone pathologies. In Section 3 we present the high-level specification of bone remodeling in the language of the Shape Calculus. In Section 4 we describe the stochastic agent-based simulator. In Section 5, we analyze and validate the results of the simulation, comparing healthy and pathological scenarios. Conclusions are given in Section 6.

2 Dynamics of Bone Remodeling

Bone remodeling is a process which iterates throughout life and it consists of two main phases: bone resorption and bone formation. Bone homeostasis is one of the most important requirements in the BR system, since pathologies typically arise when resorption and formation are not well-balanced: osteoporosis is an example of negative remodeling where resorption prevails on formation. In this situation even small negative changes in bone density are greatly amplified after several remodeling iterations. The BR system consists of multiple dynamic and interacting components, the bone cells. *Osteoclasts* ("the diggers") and *osteoblasts* ("the fillers"), form together the so-called *Basic Multi-cellular Units (BMUs)*. Another type of cells, the *osteocytes*, plays a relevant role in the remodeling process. They are located in the bone matrix and are interconnected through the *canalicular network*. Osteocytes control the BMU activity, serving as mechanosensors: load-induced signals from the tissue level are transmitted at cellular level to activate bone remodeling. This process is generally referred as *mechanotransduction*. Therefore osteocytes' signaling and RANK/RANKL/OPG signaling introduced in Section 1 represent the main communication protocols between the components of the BR system.

There are two main types of bone: *compact* (or cortical) tissue that forms the outer shell of bones, consisting of a very hard mass of bony tissue arranged in concentric layers (Haversian systems); *trabecular* (also known as cancellous or "spongy") tissue that is located beneath the compact bone and consists of a meshwork of bony bars (*trabeculae*) with many interconnecting spaces containing bone marrow. The key events occurring during a regular BR cycle are:

- **Origination.** After a micro-crack, or as a response to mechanical stress, the osteocytes in the bone matrix start producing biochemical signals towards the surface cells around the bone, termed *lining cells*. The lining cells pull away from the bone matrix, forming a canopy which merges with the blood vessels.
- **Osteoclast recruitment.** Stromal cells divide and differentiate into osteoblasts precursors. Pre-osteoblasts start to express RANKL, attracting pre-osteoclasts, which have RANK receptors on their surfaces. RANK/RANKL signaling triggers pre-osteoclasts' proliferation and differentiation.
- **Resorption.** The pre-osteoclasts enlarge and fuse into mature osteoclasts. In cortical BMUs, osteoclasts excavate cylindrical tunnels in the predominant loading direction of the bone, while in trabecular bone they act at the bone surface, digging a trench rather than a tunnel. After the resorption process has terminated, osteoclasts undergo apoptosis.
- **Osteoblast recruitment.** Pre-osteoblasts mature into osteoblasts and start producing OPG. OPG inhibits RANKL expression, and consequently protects bone from excessive resorption since it avoids other osteoclasts from being recruited by RANK/RANKL binding.
- **Formation.** Osteoblasts fill the cavity by secreting layers of osteoid. Once the complete mineralization of the renewed tissue is reached, some osteoblasts can go into apoptosis, while other can turn into lining cells or remain trapped in the bone matrix and become osteocytes.
- **Resting.** The damage has been repaired and the initial situation is re-established.

The RANK/RANKL/OPG pathway (Fig. 1) prominently affects the outcome of the BR process. Indeed, RANK/RANKL signaling induces osteoclasts' differentiation and proliferation, so that higher concentrations of RANKL lead to a higher production of osteoclasts and in turn to a higher resorption activity. In principle an overproduction of RANKL, which is indicative of an inflammation or of hormonal imbalance, does not directly give rise to osteoporosis: in young patients an unexpected high resorption activity can be well-balanced by a proper number of osteoblasts. However, in older people cellular activity is typically less effective in terms of resorption and formation rates. When combining high RANKL values with aging factors, a higher resorption activity promoted by RANKL cannot be balanced by the available osteoblasts. This configuration would give rise to negative remodeling phenomena and after several remodeling cycles during which the bone mass keeps constantly decreasing, to defective bone diseases like osteoporosis.

2.1 Related work

In the last twenty years, a variety of mathematical models has been proposed in order to better understand the dynamics of bone remodeling (reviewed in [8], [9], [10]). Early models were focused on the organ level, and they typically describe bone as a continuum material only characterized by its density. Bone micro-structure is not taken into account, thus ignoring structural adaptation mechanisms as well as complex cellular-level dynamics. Therefore in continuum-based organ-level models the differences between cortical and trabecular bone were just in their apparent density. In order to address the lack of micro-structural information, later models started looking at the biomechanical properties of the bone tissue that is, how mechanical loading affects the tissue structure and consequently its function. Models describing the mechanical response and adaptation of bone typically rely on *Finite Element Methods (FEM)* [11], a technique borrowed from the engineering community. In this case, bone adaptation is often modeled as a structural optimization problem: a FEM analysis computes the

mechanical stresses at each location of the bone matrix; then, structural changes are driven in order to optimize the homogeneous distribution of mechanical loading, until a remodeling equilibrium is reached. Another class of models describe the single-cellular and multi-cellular level and the interactions occurring among the different types of bone cells involved in the BR process. Most of these models analyze the continuous variations in the number of bone cells, and the bone density is usually calculated as a function of the number of osteoblasts and osteoclasts and their formation and resorption rates. These models can also incorporate intracellular signaling pathways and mechanosensing mechanisms, that is the process by which mechanical stimuli are transduced into cellular signals.

Despite most of the current efforts in the modeling of the BR process rely on continuous mathematics (i.e. differential equations models), in this work we exploit computational models, regarding the bone remodeling system as a *reactive concurrent system* [12]. Bone cells are modeled as processes that continuously *react* with each other by emitting and sensing molecular signals (RANK/RANKL/OPG signaling), and *concurrently* operate and access to shared resources (i.e. the bone).

Computational bone remodeling is a research field of increasing interest and there are several recent works worth mentioning. In [13] the mechanism of bone remodeling inspires a structural optimization algorithm which combines a FEM analysis with Cellular Automata; [14] defines a Petri Net model for BR; in [15] a particular class of membrane systems are used to describe the BMU dynamics; finally in [16] probabilistic verification techniques are employed in order to assess bone pathologies over a stochastic model of bone remodeling.

In the next section we will discuss the importance of capturing spatial and physical features of biological systems, and we will provide a computational model for bone remodeling, described in the process algebraic language of the Shape Calculus.

3 Bone remodeling in the Shape Calculus

In this section we firstly introduce the *Shape Calculus* [5], [6] a spatial process calculus for modeling biological and cyberphysical systems, in which the classical notion of process is enriched with features like mass, position, velocity, shape, collision, binding, and splitting. Secondly we give a high-level formal description of the spatial and multiscale dynamics of bone remodeling, by employing the Shape Calculus as a specification language.

Current research trends in cellular biology are giving a crucial role to spatial organization and location, in other words to the *spatial cell biology*. Indeed spatial organization and location prominently affect the behavior, the development and the evolution of biological entities: they occupy a certain space; they move and interact with their spatial neighbors; they express signals which propagate within a particular distance; and their internal spatial organization and their shape regulates their functionalities. The dynamics of bone remodeling exhibits spatial and geometrical properties. For instance, the amount of resorbed bone depends on the surface extension of osteoclasts, which have ruffled borders functional to resorption; osteocytes sense micro-fractures due to the apoptosis of the cells close to it; and abnormalities in bone size and shape may underlie pathological conditions.

Many computational formalisms equipped with spatial capabilities have been proposed so far (see [17] for an exhaustive review). In the field of process algebras, compartmentalization is a common way to represent process localization [18], [19], [20]. Recent works address the problem of expressing also more complex spatial features [21], [22], [23], by considering physical information, position and movement in discrete or continuous coordinate systems, geometry and geometrical transformations. The Shape Calculus features a rich set of spatial and physical primitives and being particularly suitable for describing cellular mechanisms as well as molecular signaling, it could help in giving a deeper understanding of the spatial aspects involved in the process of bone remodeling.

3.1 Overview of the calculus

The building blocks of the Shape Calculus are the so-called 3D processes which move, collide and interact in the 3D space. A 3D process is characterized by an *internal behavior* B specified in a timed variant of *CCS (Calculus of Communicating Systems)* [24]; and by a *3D shape* S, that defines the geometry and the physical properties of the process. $S[B]$ denotes a 3D process with behavior B and shape S. As in [3], [4], the syntax of the calculus, given in Table 3.1, includes additional terms for expressing repeating behaviors (*iteration*), removal of a 3D shape (*thanatos*), and time-bounded behaviors (*duration*).

The set $\mathbb{S}$ of **3D shapes** is composed of basic shapes σ, defined as a tuple $\sigma = \langle V, m, \mathbf{p}, \mathbf{v} \rangle$ (geometry, mass, position, velocity); and by compound shapes of the form $S_1\langle X \rangle S_2$, resulting from the binding of two 3D shapes S_1 and S_2 on a common surface X. Shapes move according to their velocities that are determined by a general motion law - for instance as in a force field or Brownian motion - and by the collisions occurring among shapes.

The internal **behavior** of a 3D process supports *bind* actions, with which processes can bind together forming a compound new process; and *split* actions for breaking bonds. The binding between 3D processes is modeled in a similar way to CCS communication

$S ::=$		**3D shape** ($\mathbb{S}$-term)
	$\sigma = \langle V, m, \mathbf{p}, \mathbf{v} \rangle$	Basic shape
	$S\langle X \rangle S$	Composed shape
$B ::=$		**Behavior** ($\mathbb{B}$-term)
	nil	Null behavior
	$\langle \alpha, X \rangle.B$	Bind
	$\omega(\alpha, X).B$	Weak split
	$\rho(L).B$	Strong split
	$\epsilon(t).B$	Delay
	$B + B$	Choice
	$(B)^k.B$	Iteration
	$\Theta.B$	Thanatos
	$\delta(t, B).B$	Duration
	K	Process name
$P ::=$		**3D process** (3DP-term)
	$S[B]$	$S \in \mathbb{S}, B \in \mathbb{B}$
	$P\langle a, X \rangle P$	Composed 3D process
$N ::=$		**3D network** ($\mathbb{N}$-term)
	nil	Empty network
	P	$P \in$ 3DP
	$N \| N$	Parallel 3D processes

TABLE 1
Shape Calculus syntax

on complementary channels; in the Shape Calculus, channels act as binding sites and are of the form $\langle \alpha, X \rangle$, where α is a channel name, and X is the active surface. The set of channels is denoted with $\mathcal{C}$. Binding between two processes occurs if they expose *compatible* channels. Two channels $c_1 = \langle \alpha, X \rangle, c_2 = \langle \beta, Y \rangle \in \mathcal{C}$ are said *compatible* (written $c_1 \sim c_2$), if they have complementary channel names: $\alpha = \overline{\beta}$; and they share a common surface of contact: $X \cap Y \neq \emptyset$. In addition, the Shape Calculus supports two basic actions for splitting an established bond: the *weak-split* $\omega(\alpha, X)$ (not-urgent, can be postponed) and the *strong-split* $\rho(L), L \subseteq \mathcal{C}$ (urgent, must be performed as soon as it is enabled). The sets of weak-split actions and strong-split actions are denoted with $\omega(\mathcal{C}) = \{\omega(\alpha, X) | \langle \alpha, X \rangle \in \mathcal{C}\}$, and $\rho(\mathcal{C}) = \{\rho(\alpha, X) | \langle \alpha, X \rangle \in \mathcal{C}\}$, respectively.

The term $(B)^k$ is a syntactical construct for expressing behaviors repeating for a finite ($B^n,\ n \in \mathbb{N}$) or infinite (B^∞) number of iterations. The behavioral term Θ, or *Thanatos*, removes a 3D shape from the network. Even when the behavior B of a 3D process $S[B]$ reaches the termination state nil, the associated shape S would keep existing, moving and (elastically) colliding. By performing a Θ before the behavior termination ($B \stackrel{\text{def}}{=} B_1.\Theta.B_2$), we ensure that the associated 3D shape will not affect the other processes that are concurrently executing. The term $\delta(t, B)$ called *behavior duration* allows us to express time-bounded behaviors, for instance an osteoblast that continuously mineralizes bone until its life time has passed. It has the following meaning: while $t > 0$, $\delta(t, B) \equiv B$; once $t = 0$, $\delta(t, B) \equiv \mathsf{nil}$.

The set 3DP of **3D processes** is composed of basic processes of the form $S[B]$, which are characterized by a behavior $B \in \mathbb{B}$ encapsulated in a 3D shape $S \in \mathbb{S}$; and by composed processes $P_1\langle a, X \rangle P_2$, where $P_1, P_2 \in$ 3DP, a is the name of the two compatible channels, and X is the common surface of contact.

Finally, we define a **network of 3D processes** (3D network, for short) as the parallel composition of zero or more 3D processes. Given a finite set of indexes $I = \{1, \ldots, n\}$, we can alternatively write $(\|P_i)_{i \in I}$ or $(\|P_i)_{i=1}^n$, with $P_i \in$ 3DP, to denote the network that consists of all P_i with $i \in I$: $P_1 \| \ldots \| P_n$.

In detail, the semantics of the calculus is given in Appendix A. The language presented in this work includes some new features with respect to the original formulation of the Shape Calculus. In this way we substantially improve the expressiveness of the calculus, with terms of practical usefulness (*Iteration*) and terms driven by biological evidence (*Thanatos* and *Duration*). We refer the interested reader also to papers [5], [6] for a broader view of the original formulation of the calculus.

3.1.1 A key application

In this part we give an idea of the semantics of the Shape Calculus through the example in Fig. 3: the OPG inhibition of RANKL, also discussed in the previous sections.

Consider two 3D processes: a pre-osteoblasts $Pb \stackrel{\text{def}}{=} S_{Ob}[\mathsf{B_{Pb}}]$, and a mature osteoblast $Ob \stackrel{\text{def}}{=} S_{Ob}[\mathsf{B_{OPG}}]$, where $\mathsf{B_{Pb}} \stackrel{\text{def}}{=} \langle \overline{\mathsf{rankl}}, \mathsf{X_1} \rangle.\rho(\overline{\mathsf{rankl}}, \mathsf{X_1}).\mathsf{B_{OPG}}$; $\mathsf{B_{OPG}} \stackrel{\text{def}}{=} \langle \mathsf{rankl}, \mathsf{X_2} \rangle.\rho(\mathsf{rankl}, \mathsf{X_2}).\mathsf{B_{Ob}}$; and $\mathsf{B_{Ob}}$ is the behavior of an active osteoblast which forms new bone. Pb expresses RANKL by exposing the output channel $\langle \overline{\mathsf{rankl}}, \mathsf{X_1} \rangle$; Ob expresses the decoy receptor OPG, here implemented as the input channel $\langle \mathsf{rankl}, \mathsf{X_2} \rangle$. We assume that the exposed surfaces $\mathsf{X_1}$ and $\mathsf{X_2}$ correspond to the whole surface of S_{Ob}. If $\mathsf{X_1}$ and $\mathsf{X_2}$ come into contact, i.e. $X_1 \cap X_2 \neq \emptyset$, the channels $\langle \overline{\mathsf{rankl}}, \mathsf{X_1} \rangle$ and $\langle \mathsf{rankl}, \mathsf{X_2} \rangle$ will become compatible. Consequently, the two processes bind together mimicking the RANKL/OPG binding, and the resulting compound process is $S_{Ob}[\rho(\overline{\mathsf{rankl}}, \mathsf{X_1}).\mathsf{B_{OPG}}]\langle \mathsf{rankl}, \mathsf{Y} \rangle S_{Ob}[\rho(\mathsf{rankl}, \mathsf{X_2}).\mathsf{B_{Ob}}]$, where $Y = X_1 \cap X_2$. At this point, both processes can perform a split on the established bond, written $Pb \xrightarrow{\rho(\overline{\mathsf{rankl}}, \mathsf{X_1})}$ and $Ob \xrightarrow{\rho(\mathsf{rankl}, \mathsf{X_2})}$. When the split is fired, the resulting 3D network will be $S_{Ob}[\mathsf{B_{OPG}}] \ \| \ S_{Ob}[\mathsf{B_{Ob}}]$. In a few words the above described model of RANKL/OPG binding implements a reaction from a pair *(pre-osteoblast, mature osteoblast)* to a pair *(mature osteoblast, active osteoblast)*.

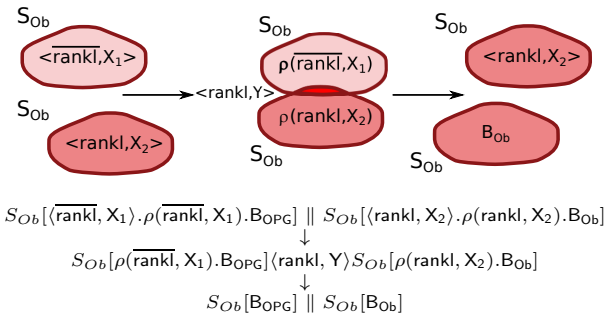

Fig. 3. RANKL/OPG signaling in the Shape Calculus. The pre-osteoblast expresses RANKL ($\langle \overline{\text{rankl}}, X_1 \rangle$) and the mature osteoblast expresses OPG ($\langle \text{rankl}, X_2 \rangle$). By binding and splitting on $\langle \text{rankl}, \cdot \rangle$, the mature osteoblast inhibits the pre-osteoclast which subsequently starts producing OPG as well. The example models a reaction *(pre-osteoblast, mature osteoblast)* $\rightarrow$ *(mature osteoblast, active osteoblast)*.

3.2 Formal specification of bone remodeling

In Table 2, the high-level Shape Calculus specification of bone remodeling is presented. Employing the Shape Calculus as a specification language has a twofold benefit:

- *Multiscale expressiveness.* The algebraic approach is able to span different scales in a compositional way: a BMU is defined in terms of a network of bone cells, and the bone tissue in terms of a network of BMUs.
- *Biological meaningfulness.* The specification follows the paradigm of *Processes as cells* and *Channels as Molecular Signals*. As a matter of fact, cells communicate with each other via direct contact (or over short distances). Similarly in the Shape Calculus, 3D processes communicate by binding on a common surface of contact. Furthermore RANK, RANKL and OPG are surface-bound proteins and consequently can be faithfully described by Shape Calculus channels of the form $\langle a, X \rangle$, where X is a portion of the surface of the associated process (i.e. a cell).

In this context, the model does not define particular binding surfaces for the channels exposed by the 3D processes, but we assume that their whole surface is available for binding for two main reasons. Firstly, there is no clear experimental evidence of the positioning of the RANK and RANKL (implemented as Shape Calculus channels) molecules at the cell surface. Secondly, the definition of a precise geometry for molecular channels would have restricted the binding capabilities of the bone cells, without any biological motivation. Let $\mathcal{B}(S)$ be the boundaries of a shape S; for the sake of succinctness, in our specification we will denote the channel $\langle \alpha, \mathcal{B}(S) \rangle$ with $\langle \alpha, X \rangle$.

In addition there are two particular actions not encoded as behavioral terms, **resorb** and **form**. They are timed action responsible for decreasing/increasing the density of the part of bone which the osteoclast/osteoblast is attached to, according to determined resorption/formation rates. These two terms have been left unimplemented at this level in order to avoid unnecessary and inaccurate modeling artifacts. Indeed it would be quite inopportune to express the bone mass as a 3D process, and moreover the activities of resorption and formation cannot be properly described by a binding operation. The quantitative parameters of the model are summarized in Table 3.

4 Stochastic Agent-Based Simulator

Traditionally, Systems Biology has been described by using continuous deterministic mathematical models like ODEs and PDEs. A growing amount of experimental results is nowadays showing that biochemical kinetics at the single-cell level are intrinsically stochastic, suggesting that stochastic models are more effective in capturing the multiple sources of heterogeneity needed for modeling a biological dynamical system in a realistic way. In particular biological systems have also developed strategies for both exploiting and suppressing biological noise and heterogeneity.

Similarly the process of bone remodeling exhibits stochastic features. The statistical fluctuations in RANKL concentrations in the blood micro-circulation produce changes in the chemotaxis, i.e. the process by which cells move toward attractant molecules, of osteoclasts and osteoblasts (for example, the cell differentiation, number and arrival time). Other important sources of variability are related to the time and space organization of the BMU; the availability of molecules required for building the bone; the regulatory feedback control and the mechanical boundary conditions [25]. In this part we address the need for such quantitative information in order to enrich the qualitative description of bone remodeling provided with the Shape Calculus in Section 3. So far few efforts have been made in characterizing the stochastic dynamics of bone remodeling, and we have recently investigated this research direction in [16], where a stochastic model for cellular bone remodeling is presented and probabilistic verification techniques are employed to assess particular bone pathologies.

In this section we describe the implementation level of our modeling framework (as introduced in Section 1), that is an agent-based simulator for Shape Calculus specifications featuring stochastic actions and perception. In particular we have developed a library to support the definition of *agents as 3D processes*, providing a rigorous translation of Shape Calculus specifications into agent code (see Appendix B for the details on the translation function). Parameters for the Shape Calculus model and for the simulator are listed in Table 3. Table 4 shows an example where the algebraic specification of an osteocyte is translated into agent code.

Tissue, BMU

$Tissue$	$\stackrel{\text{def}}{=}$	$(\|ABMU_i)_{i=1}^{a} \parallel (\|QBMU_j)_{j=1}^{q}$
BMU_a	$\stackrel{\text{def}}{=}$	$(\|Oy_i)_{i=1}^{n_{Oy}} \parallel (\|Oc_j)_{j=1}^{n_{Oc}} \parallel (\|Ob_k)_{k=1}^{n_{Ob}}$
BMU_q	$\stackrel{\text{def}}{=}$	$(\|Oy_i)_{i=1}^{n_{Oy}}$

Bone tissue is structured in a active BMUs (BMU_a) participating in the remodeling process, and in q quiescent BMUs (BMU_q). Each active BMU is in turn composed by n_{Oy} osteocytes, n_{Oc} osteoclasts and n_{Ob} osteoblasts. An inactive BMU is modeled as a network of only osteocytes.

Osteocyte

Oy	$\stackrel{\text{def}}{=}$	$S_{Oy}[(\langle \mathsf{can}, \mathsf{X}\rangle + \langle \overline{\mathsf{can}}, \mathsf{X}\rangle)^{\mathsf{k_{Oy}}} + \langle \overline{\mathsf{oySig}}, \mathsf{X}\rangle.\Theta]$

An osteocyte can bind with other $\mathsf{k_{Oy}}$ osteocytes through the channel $\langle \mathsf{can}, \cdot\rangle$ and form the network of canaliculi. Alternatively, if they are not near enough to communicate and bind with each other, e.g. osteocytes near the bone surface, they expose the channel $\langle \overline{\mathsf{oySig}}, \cdot\rangle$ modeling the osteocytes' signaling that will activate the resorption phase and the remodeling process. After having performed a bind on $\langle \mathsf{oySig}, \cdot\rangle$, the osteocyte dies since it has been consumed by the attached osteoclast.

Osteoclast

Oc	$\stackrel{\text{def}}{=}$	$S_{Oc}[\mathsf{B_{Oc}}]$
$\mathsf{B_{Oc}}$	$\stackrel{\text{def}}{=}$	$\delta(\mathsf{t_{Oc}}, \mathsf{B_{AOc}}).\Theta.\langle \overline{\mathsf{deathF}}, \mathsf{X}\rangle^{\mathsf{k_{Oc}}}$
$\mathsf{B_{AOc}}$	$\stackrel{\text{def}}{=}$	$(\langle \mathsf{oySig}, \mathsf{X}\rangle + \langle \mathsf{rankl}, \mathsf{X}\rangle.\rho(\mathsf{rankl}, \mathsf{X})).\mathbf{resorb}$

During its lifetime $\mathsf{t_{Oc}}$, an osteoclast behaves as an active osteoclast ($\mathsf{B_{AOc}}$): it continuously absorbs bone, induced by osteocytes' signaling (channel $\langle \mathsf{oySig}, \cdot\rangle$) or by RANKL (channel $\langle \mathsf{rankl}, \cdot\rangle$). Before dying, it releases death factors that will attract osteoblasts to the consumed part of bone, thus triggering the formation phase. In particular, a single "dead" osteoclast can bind with $k_{Oc} = \lfloor \mathsf{n_{Ob}}/\mathsf{n_{Oc}} \rfloor$ osteoblasts, so fitting the ratio between active osteoclasts and active osteoblasts.

Osteoblast

Ob	$\stackrel{\text{def}}{=}$	$S_{Ob}[\langle \overline{\mathsf{rankl}}, \mathsf{X}\rangle.\rho(\overline{\mathsf{rankl}}, \mathsf{X}).\mathsf{B_{OPG}} + \epsilon(\mathsf{t_{Pb}}).\mathsf{B_{OPG}}]$
$\mathsf{B_{OPG}}$	$\stackrel{\text{def}}{=}$	$\langle \mathsf{rankl}, \mathsf{X}\rangle.\rho(\mathsf{rankl}, \mathsf{X}).\mathsf{B_{Ob}} + \mathsf{B_{Ob}}$
$\mathsf{B_{Ob}}$	$\stackrel{\text{def}}{=}$	$\delta(\mathsf{t_{Ob}}, \langle \mathsf{deathF}, \mathsf{X}\rangle.\mathbf{form}).\Theta$

An osteoblast initially behaves as a non differentiated cell: it produces RANKL, by exposing channel $\langle \overline{\mathsf{rankl}}, \cdot\rangle$. After the effect of OPG-inhibition or after its differentiation time $\mathsf{t_{Pb}}$ has elapsed, it starts behaving as a mature osteoblast which produces OPG. In particular, a mature osteoblast can inhibit a single precursor, by binding on the channel $\langle \mathsf{rankl}, \cdot\rangle$ (standing for the OPG decoy receptor) (Fig. 3). Then, the formation phase lasts a time $\mathsf{t_{Ob}}$, after which the cell undergoes apoptosis.

TABLE 2
Shape Calculus specification and biological description of bone remodeling.

Param	Value	Description
$\mathsf{n_{Oc}}$	20 [26], [27]	Expected number of Oc
$\mathsf{n_{Ob}}$	2000 [26], [27]	Expected number of Ob
$\mathsf{t_{Oc}}$	10 days [27]	Oc lifetime
$\mathsf{t_{Ob}}$	15 days [27]	Mature Ob lifetime
$\mathsf{t_{Pb}}$	5 days [27]	Ob differentiation time
$\mathsf{size_{BMU}}$	$2.4\times1.6\times0.01$ mm^3 [27]	Size of the BMU
$\Delta\mathsf{t}$	1 day	Time step
$\mathsf{k_{Oc}}$	2.5 days^{-1}	Resorption rate
$\mathsf{k_{Ob}}$	0.25 days^{-1}	Formation rate
$\mathsf{k_{RANKL}}$	$\in [1, 2]$	RANKL factor
$\mathsf{k_{aging}}$	$\in [1, 2]$	Aging factor
$\mathsf{d_{Oc-Oy}}$	0.06 mm	Oc perception radius to Oy
$\mathsf{d_{Pb-Oc}}$	0.01 mm	Pb perception to Oc death factor
$\mathsf{d_{Ob-Pb}}$	0.01 mm	Ob/OPG perception to Pb/RANKL
$\mathsf{D_{Oc}}$	10^{-2} mm^2/day	Oc diffusion coefficent
$\mathsf{D_{Ob}}$	2.15×10^{-2} mm^2/day	Ob diffusion coefficent

TABLE 3
Model parameters. Size of the BMU, lifetime and expected concentration of bone cells have been taken from literature. Other parameters have been estimated from the model (see Appendix C).

$$Oy \stackrel{\text{def}}{=} S_{Oy}[(\langle \mathsf{can}, \mathsf{X}_1\rangle + \langle \overline{\mathsf{can}}, \mathsf{X}_2\rangle)^{\mathsf{k_{Oy}}} + \langle \overline{\mathsf{oySig}}, \mathsf{X}_3\rangle.\Theta],$$
$$S_{Oy} = \langle V_{Oy}, m_{Oy}, \mathbf{p}_{Oy}, \mathbf{v}_{Oy}\rangle$$
$$\downarrow$$

```
Channel c1 = new InChannel("can", X_1, prob);
Channel c2 = new OutChannel("can", X_2, rate1, d1);
Channel c3 = new OutChannel("oySig", X_3, rate2, d2);
Behaviour b1, b2, b3, b4;
b1 = new Choice(new Bind(c1), new Bind(c2));
b2 = new Iteration(b1, k_Oy);
b3 = new Sequence(new Bind(c3), new Thanatos());
b4 = new Choice(b2,b3);
Shape oy = new BasicShape(m_Oy, p_Oy, v_Oy, b4);
```

TABLE 4
Example of translation from a Shape Calculus term describing an osteocyte into agent code.

Shape Calculus-based agents have associated two further features: *stochasticity*, that enriches agents' actions with stochastic rates modeling the propensity of the action itself; and *perception*, that is the capability to communicate at distance and sense the neighborhood.

Stochasticity. We follow the so-called *rated output/passive input approach* [28], where agent actions are equipped with *stochastic rates* and *weights*. In particular, *output actions* are annotated with a rate $\lambda \in \mathbb{R}^+$, while *input actions* have associated a weight $w \in \mathbb{N}^+$, representing the probability that the specific input is selected when a compatible output action is fired. Consider the system in Figure 4, where two agents $\mathcal{A}$ and $\mathcal{B}$ are illustrated. Agent $\mathcal{A}$ can perform an output action $\overline{a}$ with rate λ; while $\mathcal{B}$ can perform the input actions (a, w_1) and (a, w_2). The relative

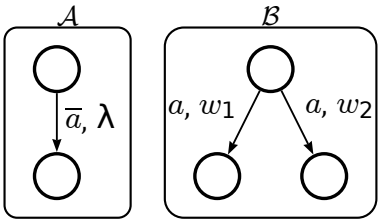

Fig. 4. Agents synchronizing on compatible channels with stochastic rate λ and probability w_i.

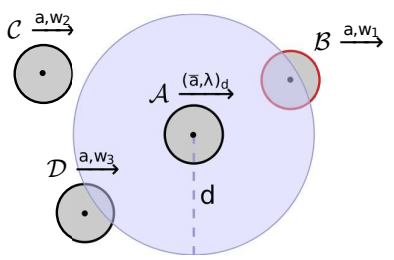

Fig. 5. Agents exposing binding capabilities. Agents $\mathcal{C}$ and $\mathcal{D}$ is out of the perception radius of $\mathcal{A}$ (the blue circle), determined by the sensibility distance d. On the other hand, $\mathcal{A}$ can detect and bind with agent $\mathcal{B}$ because its center is within the perception radius of $\mathcal{A}$.

selection probability of action (a, w_i), called $p(a, w_i)$, is calculated as the ratio between w_i and the total weight of a, that is the sum of the weights of all the enabled a-actions; in this example,

$$p(a, w_i) = \frac{w_i}{w_1 + w_2}, \ i = 1, 2.$$

Then, the *synchronization rate* between the actions (a, w_i) and $(\overline{a}, \lambda)$ is given by $\lambda \cdot p(a, \omega_i)$.

Perception. Differently from the theory of the Shape Calculus where binding between two 3D processes can exclusively occur when they share a common surface of contact, we allow compatible agents to bind at distance, according to a given perception radius. More precisely, output bind actions are annotated with a parameter $d \in \mathbb{R}^+$ called *sensibility distance*, meaning that if an agent $\mathcal{A}$ can perform an action $(\overline{a}, \lambda)_d$, it can bind with any agent $\mathcal{B}$ which can perform a compatible action (a, w) and which is distant from $\mathcal{A}$ at most d. Figure 5 depicts a situation where an agent $\mathcal{A}$ is able to execute an output bind action $(\overline{a}, \lambda)_d$. Even if agents $\mathcal{C}$ and $\mathcal{D}$ expose complementary channels, they are out of the perception radius of $\mathcal{A}$, which can consequently bind only with agent $\mathcal{B}$. The actual distance between two agents affects their synchronization rate, as expected, since longer distances should lead to longer action durations and consequently to lower rates. Therefore, we define the *binding rate* between two compatible bind actions $(\overline{a}, \lambda)_d$ and (a, w) exposed by agents $\mathcal{A}$ and $\mathcal{B}$ respectively, by the ratio $\frac{\lambda \cdot p(a, \omega)}{d(\mathcal{A}, \mathcal{B})}$, where $d(\mathcal{A}, \mathcal{B})$ is the distance between $\mathcal{A}$ and $\mathcal{B}$.

The simulator is based on the *Repast Symphony Suite* [29], an agent-based modeling and simulation (ABMS) toolkit in Java [1]. Figure 6 shows a screen-shot taken during a simulation. The simulator allows us to visualize at runtime the location of bone cells in the BMU, the bone density and micro-structure, and the spatial diffusion of RANKL. Furthermore it supports several runtime plots including bone mineral density, resorption and formation activities, RANKL concentration and number of active/total bone cells.

Repast models are based on the concept of *context*, which is a structured container serving as the agents' environment. A context may include one or more *projections*, that represent the spatial domains where agents are located (for example, continuous and discrete spaces). A projection in turn can have associated *value layers*, i.e. spatial data structures holding a numerical value for each position, and that can be accessed by agents. Simulations in Repast are based on a discrete-event execution model, where time proceeds by discrete steps, called *ticks* and actions are scheduled for the execution at a specific tick. In the following we provide some details on the various components of the agent-based model.

Computation model. Repast implements the discrete-event computation model through a scheduler holding a list of pending actions as $(action, tick)$ couples. At each tick t all the actions (a, t) are executed. This execution model adapts well to the simulation algorithm defined in the theory of the Shape Calculus [5], [6], where the time-line is divided in time-steps of duration Δt. After each Δt the velocities and the positions of all the shapes are updated, according to their particular motion law. However in the stochastic settings we must consider actions with exponentially distributed durations that are determined by the rate of the action itself. Moreover the race condition applies so that shorter actions should be executed earlier. Appendix D shows the pseudo-code implementing the stochastic scheduler. In few words, if an action has a duration less than or equal to Δt, it is performed at Δt; otherwise, it is postponed to the subsequent time step. Given that a single remodeling cycle lasts about one year and the resorption and formation processes can take months, in this model Δt is set to $1\ day$.

Projections. We consider two different spatial domains: a continuous space, and a discrete space (i.e a grid). Space is approximated in two-dimensions, and has a size of $240 \times 160 \times 10^{-4}\ mm^2$ such that each cell in the grid models a portion of size $0.01 \times 0.01\ mm^2$. According to the parameter $size_{BMU}$ in Table 3, we can ignore the depth of the BMU ($0.01\ mm$) which is much smaller than its width ($2.4\ mm$) and its height

1. A prototype version is available at http://www.cs.unicam.it/merelli/bone/

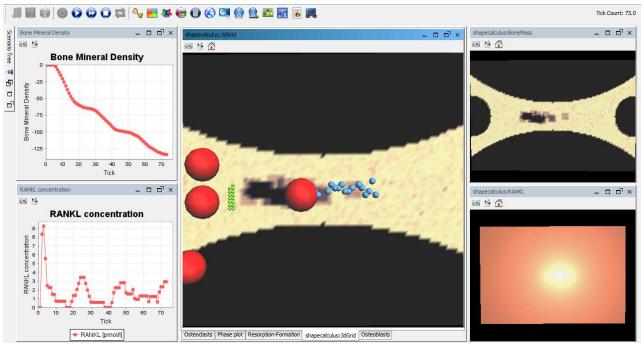

Fig. 6. Screen-shot of the agent-based simulator for bone remodeling. The center panel shows the location in the BMU of bone cells (blue: osteocytes, green: osteoblasts, red: osteoclasts). On the left side the graphs for BMD and RANKL concentration are displayed. The right panels depict the bone micro-structure and the RANKL diffusion in the BMU (brightest zones: highest concentrations).

$(1.6\ mm)$.

Bone tissue. It is modeled as a Repast value layer that is, a real-valued matrix $Bone$. The value of a cell $Bone_{ij}$ represents the percentage bone density at the position (i, j) of the BMU grid, and varies from 0 (void) to 100 (fully mineralized). The simulator supports both cortical and trabecular bone.

Molecular signals. While at the specification level molecular signals like RANKL are modeled as communication channels, at the implementation level exposed output channels are assumed to release an amount of molecules diffusing in the space. The spatial concentration of such molecules is updated at each Δt according to a *diffusion Cellular Automata* update rule [30], which corresponds to a discretization of the diffusion equation. The model considers both the RANKL signaling that affects osteoclasts' motion, so that osteoclasts are directed towards higher RANKL concentrations (attraction), and the death factors produced by osteoclasts that attract osteoblasts towards the portions of bone previously absorbed.

Cell motion. In the absence of attraction factors, an agent moves according to a random walk. At time t its position $\vec{p}(t)$ is updated by the following law (adapted from [31]):

$$\vec{p}(t + \Delta t) = \vec{p}(t) + \vec{\xi}\sqrt{2D\Delta t}$$

where ξ is a uniformly distributed random vector ranging in $[-1, 1]$, and D is the diffusion coefficient of the agent.

In the case that a cell is also affected by attraction factors, like RANKL-attracted osteoclasts, its motion is determined by a *biased random walk*, i.e. a random walk altered by the concentration gradient of an attractant molecule u. Assuming that $\vec{p}(t) = (x, y)$, let $u_{\lfloor x \rfloor, \lfloor y \rfloor}(t)$ denote the concentration of u at the discrete position $(\lfloor x \rfloor, \lfloor y \rfloor)$ and at time t. Then, the position of the agent is updated by:

$$\vec{p}(t + \Delta t) = \vec{p}(t) + \vec{\xi_{\pm}}\sqrt{2D\Delta t}$$

where now the vector $\vec{\kappa_{\pm}}$ models the "molecular bias", by taking into account the concentration gradient of u. The x coordinate of $\vec{\xi_{\pm}}$ is calculated as follows:

$$(\xi_{\pm})_x = \begin{cases} U[0,1]\dfrac{1 + u_{x^*,\lfloor y \rfloor}(t)}{1 + u_{\lfloor x \rfloor,\lfloor y \rfloor}(t)}, & \text{if } x^* \geq x \\ U[-1,0]\dfrac{1 + u_{\lfloor x \rfloor,\lfloor y \rfloor}(t)}{1 + u_{x^*,\lfloor y \rfloor}(t)}, & \text{if } x^* < x \end{cases}$$

where $U[a, b]$ is a uniformly distributed random value between a and b; x^* is the x component of the discrete position with the highest RANKL concentration in the Von Neumann neighborhood of $(\lfloor x \rfloor, \lfloor y \rfloor)$. The equivalent equation holds for $(\xi_{\pm})_y$.

Osteocytes. We assume that osteocytes produce RANKL, since osteocytes' signaling has the effect of attracting osteoclasts to the source of the signal, similarly to RANKL signaling by pre-osteoblasts. Osteocytes' initial positioning in the bone matrix is not pre-determined, and the outcome of different shapes for osteocytes' positioning is discussed in Section 5.2.

Osteoclasts. In normal conditions, the number of osteoclasts in the BMU is subject to little variations from the average $n_{Oc} = 20$. Higher perceived densities of RANKL in the environment, which are caused by an inflammation or a signaling defect, lead to a higher production of osteoclasts. Their motion law is a biased random walk affected by the RANKL concentration gradient, with a diffusion coefficient $\mathrm{D_{Oc}} = 10^{-2} mm^2/day$. The expected lifetime t_{Oc} is 10 days, but they can undergo apoptosis before t_{Oc} if a high concentration of osteoblasts is detected in the neighborhood. Having reached the portion of bone to consume, an osteoclast reduces the percentage density in that part of bone by $k_{Oc} = 2.5$ each day.

Osteoblasts. The number of osteoblasts in the system varies randomly around the average $n_{Ob} = 2000$. They move according to a biased random walk affected by the osteoclasts' death factors, with a diffusion coefficient $\mathrm{D_{Ob}} = 2.15 \times 10^{-2} mm^2/day$. Moreover, osteoblast precursors emit RANKL which contributes to osteoclasts' production and stimulation. Mature osteoblasts inhibits RANKL signaling by binding with the OPG channel. The lifetime of an osteoblast is about 20 days: 5 days as a precursor, 15 days as a mature cell active in the formation process. When active, it increases the bone density of a factor $k_{Ob} = 0.25$ each day. It can die before its lifetime has passed, if the number of active osteoclasts in the system is higher than expected.

5 RESULTS AND DISCUSSION

The aim of this work is to show how apparently insignificant changes in RANKL signaling lead to disease conditions, especially when aging factors are involved. In order to describe these two factors, we have defined two parameters, k_{RANKL} and k_{aging}, modeling respectively the effectiveness of the RANKL signaling and the aging factor in terms of a reduced cellular activity. In particular, we defined two configurations obtained by varying the parameters k_{RANKL} and k_{aging} (see Appendix C for details on parameter estimation):

- **healthy conf. ($k_{RANKL} = 1$, $k_{aging} = 1$)**, where RANKL production and cellular activity is normal;
- **osteoporotic conf. ($k_{RANKL} = 2$, $k_{aging} = 2$)**, with an overproduction of RANKL and a reduced cellular activity.

When running the osteoporotic configuration, the higher RANKL effectiveness leads to a higher production of osteoclasts, hence to a higher resorption activity. On the other hand, osteoblasts are not effective enough to completely repair the consumed bone, due to the aging factor lowering the cellular activity. This causes a lower total bone density, weaker trabeculae and consequently more frequent and more consistent micro-fractures in osteoporotic patients. It is worth noting that when the aging factor is absent, like in a young patient, an overproduction of RANKL does not determine a disease situation. Indeed, an unexpected high absorbing activity can be successfully balanced by recruiting a higher number of osteoblasts, which would not be possible in an old patient characterized by a lower cellular activity. Conversely if we consider an old patient with a regular RANKL signaling, less effective osteoclasts are balanced by less effective osteoblasts and we do not observe relevant negative remodeling phenomena.

Figure 7 groups the key snapshots taken during a simulation of one trabecular remodeling cycle, comparing the healthy and the osteoporotic configurations. We analyze the location of the cells in the BMU, the bone micro-structure, resorption and formation activities, and the RANKL concentration at time:

- $t = 150$: the first osteoblasts (green spheres) are being recruited and osteoclasts (red spheres) have almost concluded the resorption phase. Osteoblasts starts to fill the cavities excavated by osteoclasts, following them in a highly coordinated manner. At this stage, osteocytes (blue spheres) have been absorbed almost entirely. While there are no significant differences in the bone mass, we observe that RANKL concentration is higher in the osteoporotic case, as expected. This causes a faster resorption, leading in turn to a faster BMU activity, evidenced by the fact that osteoblasts are recruited earlier than in the healthy case.
- $t = 400$: the remodeling cycle is in its final days. Differences in the bone density are quite prominent: in Figure 7 (f) the cavities have almost been repaired; while Figure 7 (h) shows how the reduced osteoblastic activity generates several holes in the trabecular structure. This can be observed also in the cumulative plots of bone resorption and formation in Fig. 7 (j),(l). In healthy conditions formation (solid line) compensate resorption (dashed line), while in the osteoporotic case formation does not counterbalance resorption, even if the resorption activity is not greater than in the healthy case. In addition, we notice a lower RANKL concentration in the second half of the remodeling cycle, due to the fact that signaling osteocytes have been completely absorbed and RANKL-producing pre-osteoblasts have matured into bone-forming osteoblasts.

Figure 8 compares the bone mineral density in the healthy and in the osteoporotic case, averaged over forty runs for each configuration of a single remodeling cycle. Initial values of BMD are taken from statistical data [32] and represent the hip density of a Caucasian woman aged 25 (see Section 5.1 for a broader discussion). In normal conditions we observe that at the end of remodeling the initial bone density is reestablished, and that variations from the mean density are limited. In case of osteoporosis, the minimal values of percentage density are reached during resorption, and the final density is lower than the initial one, since the osteoblastic activity is not effective enough to counterbalance resorption. In addition, the pathological case is characterized by a higher standard deviation. However the sum of the mean density and its standard deviation at the end of remodeling is still below the optimal density, meaning that in more than the 84% of cases the outcome of bone remodeling is negative in the osteoporotic configuration.

5.1 Model Validation

In this part the outputs of the agent-based model will be validated against statistical datasets. In particular, we refer to the National Health and Nutrition Examination Survey (NHANES III, 1988-94) [32], and to hip density values taken from [33]. *Bone Mineral Density (BMD)* is an indicator of the quality of the bone and it is measured with clinical techniques, the most used of which is DEXA (Dual Energy Xray Absorptiometry). Based on BMD measurement and according to the patient's gender and ethnicity, it is possible to determine the presence of bone pathologies according to the following definitions [34]:

- *Osteopenia*, when the BMD is between 1 standard deviation (SD) and 2.5 SD below the mean of the young reference group.
- *Osteoporosis*, when the BMD is 2.5 SD or more below the mean of the young reference group.

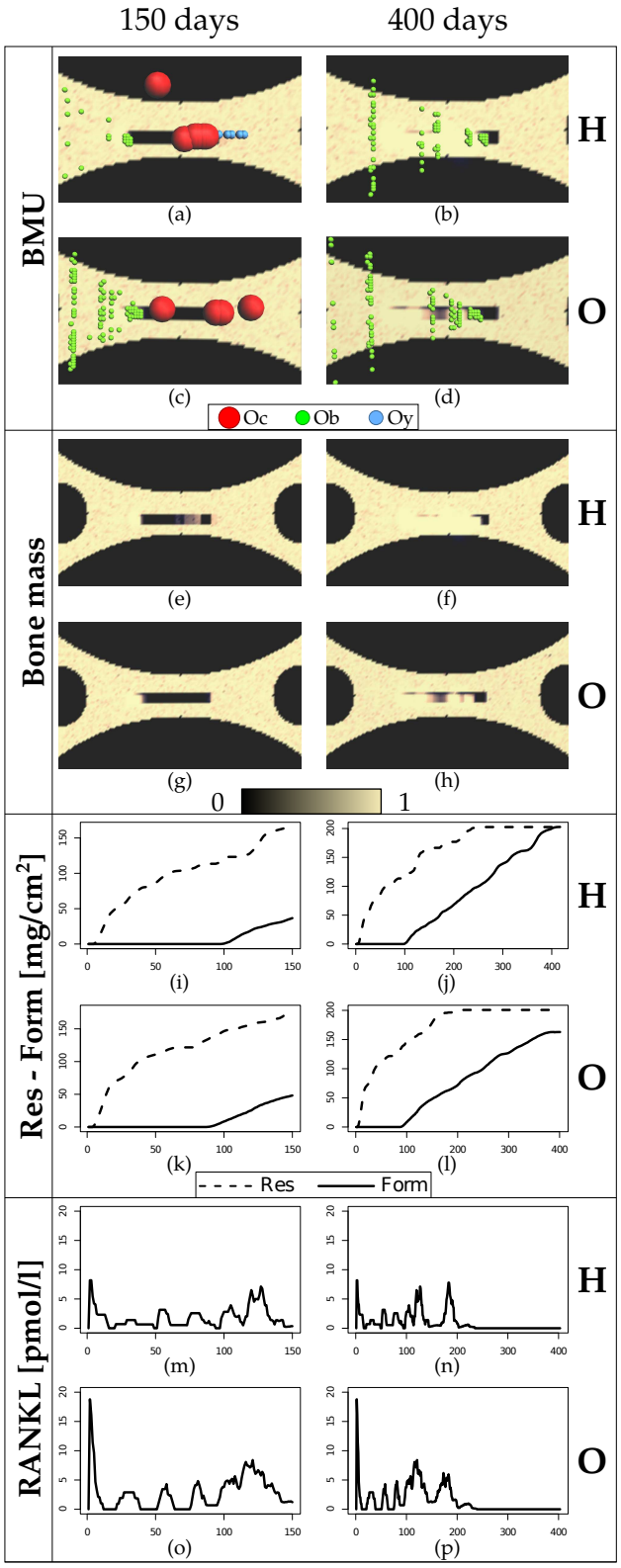

Fig. 7. Simulation of healthy (**H**) and osteoporotic (**O**) configurations. The first two rows display the position of bone cells in the BMU. The third and the fourth rows show the density of the trabecula. Graphs in the fifth and sixth row depict the cumulative values of bone resorption and formation. The last two rows show how the RANKL concentration varies during remodeling.

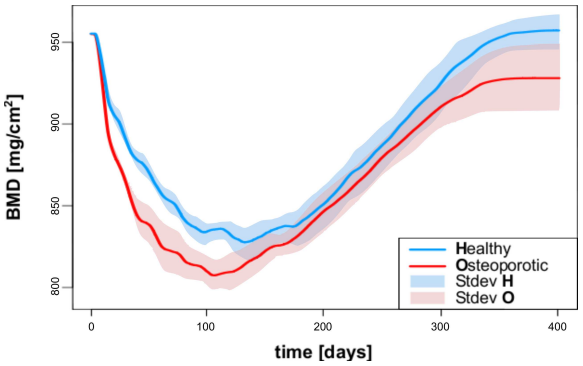

Fig. 8. Changes in BMD during one remodeling cycle. Continuous curves represent the mean density. Filled areas span the interval *mean* $\pm$ *standard deviation*. In the healthy configuration (blue curve), mineral homeostasis is maintained. On the other hand, in the pathological configuration (red curve) the final density is lower than the initial one (negative remodeling).

Therefore bone diseases are assessed by comparing the BMD measurements with statistical data obtained from population-wide surveys. Figure 9 shows the reference values for Caucasian women at about 25 years (young reference group) a), 45 years b) and 65 years c).

Simulation results show that after just one remodeling cycle both the healthy and the osteoporotic configurations return density values within the normal density range $\bar{\mu} \pm \bar{\sigma} = 955 \pm 123$, which is determined by the BMD distribution of the young reference group (see Fig. 9). After 40 simulation runs, the following results have been obtained at the end of a single remodeling cycle:

- **Healthy configuration:** $955.01 \pm 14.41 \subset \bar{\mu} \pm \bar{\sigma}$
- **Osteoporotic configuration:** $921.86 \pm 19.36 \subset \bar{\mu} \pm \bar{\sigma}$

Although in the pathological configuration we observe a lower mean density, in both cases no particular bone pathologies are diagnosed, as one can expect. Indeed it is very unlikely that pathological conditions can occur after one single remodeling cycle (corresponding to about 400 days) and starting from an optimal bone density.

As a matter of fact, osteopenia and osteoporosis are diseases resulting after several years of negative remodeling. Figure 10 plots the results of a single simulation involving seven consecutive remodeling cycles, that correspond roughly to seven years. In this case we report that when running the osteoporotic configuration, bone mineral density keeps decreasing throughout the years. At about $t = 700$ days, density reaches the range $[\bar{\mu} - 2.5\bar{\sigma}, \bar{\mu} - \bar{\sigma}]$, meaning that osteopenia would be diagnosed after less than two years. Moreover at about $t = 2100$, bone density goes below the level $\bar{\mu} - 2.5\bar{\sigma}$. Therefore running the osteoporotic configuration, osteoporosis is diagnosed after less than six years of simulation.

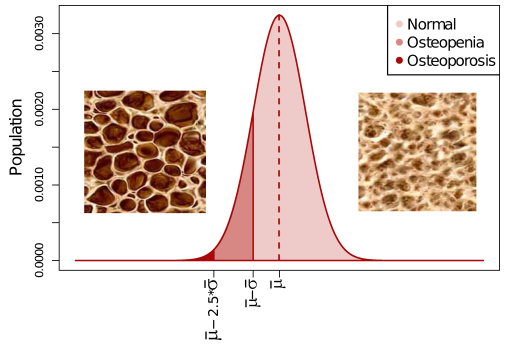

a) Caucasian women, 25 yo. $\mu = 955$ mg/cm^2; $\sigma = 123$.

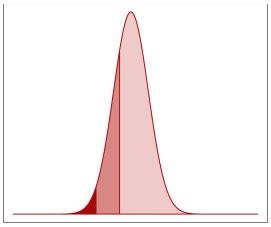

b) Caucasian women, 45 yo. $\mu = 920$ mg/cm^2; $\sigma = 136$.

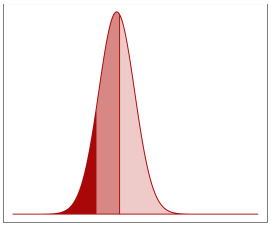

c) Caucasian women, 65 yo. $\mu = 809$ mg/cm^2; $\sigma = 140$.

Fig. 9. Hip BMD distribution in Caucasian women from statistical data in [32]. a) refers to the young reference group (25 years) with mean BMD $\bar{\mu}$ and standard deviation $\bar{\sigma}$. The filled areas below the curve and the different shades of red identify patients with normal bone, osteopenia and osteoporosis. b) and c) show the BMD distributions at 45 and 65 years respectively, where an increasing incidence of osteopenia and osteoporosis can be observed.

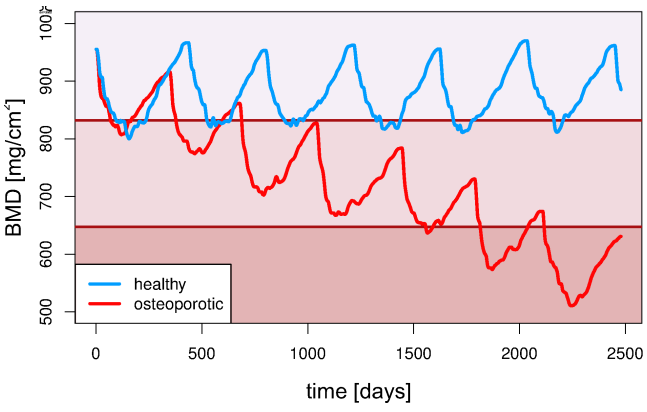

Fig. 10. Changes in BMD during seven remodeling cycles. As in Fig. 9, different shades of red determine the density ranges for normal bone, osteopenia and osteoporosis. In the healthy configuration (blue curve), the initial density is maintained after each remodeling cycle. In the osteoporotic configuration (red curve), density keeps decreasing throughout the years, going below the threshold ($\bar{\mu} - 2.5\bar{\sigma}$) under which osteoporosis is diagnosed.

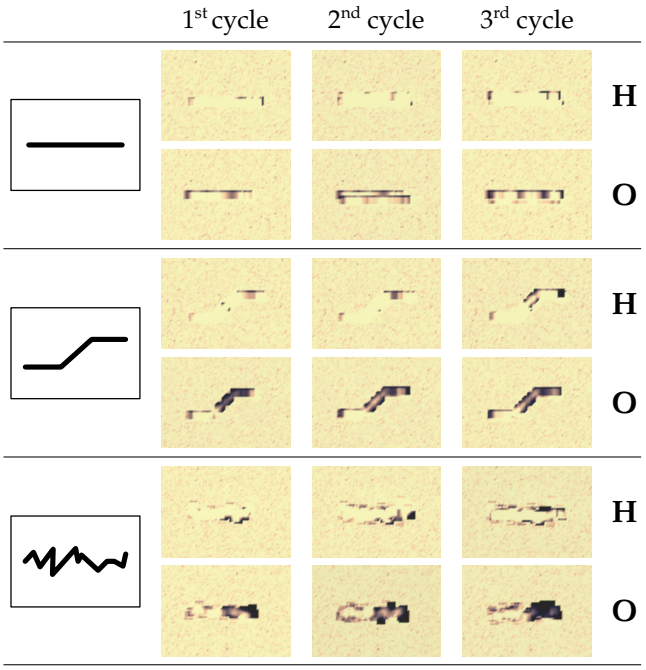

Fig. 11. The effects of different osteocytes' positioning (straight, zig-zag, and random) in the density and micro-structure of a portion of compact bone. In the healthy (**H**) case, mineral and structural homeostasis is maintained. In the osteoporotic (**O**) case, the density keeps decreasing and the structure keeps weakening.

5.2 Osteocytes' positioning affects bone micro-structure

We evaluate how the positioning of active (signaling) osteocytes affects in the long run the bone density and micro-structure. Keeping in mind that we model only signaling osteocytes, their initial positions are mainly determined by factors at tissue level. Osteocytes act as mechanosensors giving a molecular response at the cellular level to the mechanical stresses at tissue level, and they also activate along micro-fractures in the bone matrix. Considering that osteocytes are responsible for the activation of bone remodeling, this kind of analysis could explain the multiscale loop linking

1) the origination of mechanical stimuli at the tissue level, driven by the optimization of the bone micro-structure;
2) the activation of a certain number of osteocytes at a certain position in the bone matrix, determined by the entity of the mechanical stimuli;
3) depending on osteocytes' positioning, the outcome of bone remodeling in terms of updated bone density and micro-structure, which in turn triggers a new mechanical adaptation process.

Figure 11 summarizes the results obtained after three remodeling cycles, comparing healthy and osteoporotic patients and three different positioning patterns: straight, zig-zag, and random. Firstly we

observe that mineral homeostasis and bone microstructure is successfully maintained in the healthy configuration, regardless of the initial positioning of osteocytes. There are just few parts characterized by a lower density, which can be ascribed to the stochastic fluctuations in the agent-based model. Indeed, we notice that osteoblasts are able to fill any hole left in the previous remodeling cycles, but their stochastic behavior may allow some parts not to be completely repaired. On the other hand we observe a progressive micro-structural weakening in the osteoporotic configuration, so reproducing the expected defective dynamics. This qualitative analysis could be useful also in the assessment of the fracture risk in a particular osteoporotic patient, providing a more detailed and personalized scenario with respect to current medical practice that estimates the fracture risk only on a statistical basis.

6 Conclusion

In this work we have investigated the complex multiscale dynamics that connects disorders in RANKL signaling at the molecular level, to bone diseases like osteoporosis that are characterized by a lower bone mass and disruptions at tissue level. In particular our results evidence that defective bone diseases arise when a higher effectiveness of RANKL signaling is combined with aging factors reducing the activity of osteoblasts and osteoclasts. The parameters modeling the RANKL effectiveness and the aging factor have been estimated over an ODE model. By means of sensitivity analysis procedures, we have determined two configurations of parameters corresponding respectively to a healthy patient and to an osteoporotic patient. Simulation results have been validated over statistical data available from population-wide surveys. In the healthy configuration, the simulator is able to reproduce the homeostatic process of remodeling, where resorption is counterbalanced by formation. On the other hand, when the simulator is executed in the osteoporotic configuration, osteoporosis is diagnosed after less six years, even if starting from an optimal bone density. Furthermore we have looked into the connection between the spatial location of signaling osteocytes and the bone micro-structure in the long run.

From the methodological point of view, we have defined a multi-level computational framework that can be successfully employed also in other areas of biology and biomedicine. At the specification level, we describe the process of bone remodeling through a process-algebraic language, the Shape Calculus, which proved to be particularly suitable for expressing the spatial and multiscale nature of bone remodeling. At the implementation level, we have developed a stochastic agent-based simulator supporting the Shape Calculus as the model specification language (by means of translation functions); and featuring a variety of analysis and runtime monitors. We report that the stochastic agent-based simulation is time-consistent with the real biological process and that results agree with those obtained from well-established mathematical models like [26], [27].

Besides being a biomedical problem of growing importance, osteoporosis and bone remodeling are characterized by complex multiscale mechanisms not entirely explained yet, thus representing a testbed for novel modeling paradigms and techniques. The combination of formal methods with agent-based technologies has provided us with a deeper understanding of this challenging field of research and we believe that our approach could be possibly employed as a general-purpose toolkit in Computational Systems Biology.

Acknowledgments

Pietro Liò would like to thank RECOGNITION: *Relevance and cognition for self-awareness in a content-centric Internet (257756)*, funded by the European Commission within the 7^{th} Framework Programme (FP7). Nicola Paoletti would like to thank the Rizzoli Orthopaedic Institute in Bologna (IT) for funding his PhD scolarship.

References

[1] S. Jabbar, J. Drury, J. Fordham, H. Datta, R. Francis, and S. Tuck, "Osteoprotegerin, RANKL and bone turnover in postmenopausal osteoporosis," *Journal of Clinical Pathology*, vol. 64, no. 4, p. 354, 2011.

[2] N. e. a. Morabito, "Osteoprotegerin and RANKL in the Pathogenesis of Thalassemia-Induced Osteoporosis: New Pieces of the Puzzle," *Journal of Bone and Mineral Research*, vol. 19, no. 5, pp. 722–727, 2004.

[3] P. Liò, E. Merelli, N. Paoletti, and M. Viceconti, "A combined process algebraic and stochastic approach to bone remodeling," *Electronic Notes in Theoretical Computer Science*, vol. 277C, pp. 41–52, 2011.

[4] N. Paoletti, P. Liò, E. Merelli, and M. Viceconti, "Osteoporosis: a multiscale modeling viewpoint," in *Proceedings of the 9th International Conference on Computational Methods in Systems Biology*, ser. CMSB '11. ACM, 2011, pp. 183–193.

[5] E. Bartocci, D. Cacciagrano, M. Di Berardini, E. Merelli, and L. Tesei, "Timed Operational Semantics and Well-Formedness of Shape Calculus," *Scientific Annals of Computer Science*, vol. 20, 2010.

[6] E. Bartocci, F. Corradini, M. Di Berardini, E. Merelli, and L. Tesei, "Shape Calculus. A Spatial Mobile Calculus for 3D Shapes," *Scientific Annals of Computer Science*, vol. 20, 2010.

[7] L. Milanesi, P. Romano, G. Castellani, D. Remondini, and P. Liò, "Trends in modeling biomedical complex systems," *BMC bioinformatics*, vol. 10, no. Suppl 12, 2009.

[8] L. Geris, J. Vander Sloten, and H. Van Oosterwyck, "In silico biology of bone modelling and remodelling: regeneration," *Philosophical Transactions of the Royal Society A: Mathematical, Physical and Engineering Sciences*, vol. 367, no. 1895, p. 2031, 2009.

[9] F. Gerhard, D. Webster, G. van Lenthe, and R. Müller, "In silico biology of bone modelling and remodelling: adaptation," *Philosophical Transactions of the Royal Society A: Mathematical, Physical and Engineering Sciences*, vol. 367, no. 1895, p. 2011, 2009.

[10] P. Pivonka and S. Komarova, "Mathematical modeling in bone biology: From intracellular signaling to tissue mechanics," *Bone*, vol. 47, no. 2, pp. 181–189, 2010.

[11] M. Viceconti, L. Bellingeri, L. Cristofolini, and A. Toni, "A comparative study on different methods of automatic mesh generation of human femurs," *Medical engineering & physics*, vol. 20, no. 1, pp. 1–10, 1998.
[12] J. Fisher and T. Henzinger, "Executable cell biology," *Nature biotechnology*, vol. 25, no. 11, pp. 1239–1249, 2007.
[13] A. Tovar, "Bone remodeling as a hybrid cellular automaton optimization process," Ph.D. dissertation, University of Notre Dame, 2004.
[14] L. Li and H. Yokota, "Application of Petri Nets in Bone Remodeling," *Gene Regulation and Systems Biology*, vol. 3, p. 105, 2009.
[15] D. Cacciagrano, F. Corradini, E. Merelli, and L. Tesei, "Multiscale Bone Remodelling with Spatial P Systems," in *Proceedings Compendium of the Fourth Workshop on Membrane Computing and Biologically Inspired Process Calculi*, 2010.
[16] P. Liò, E. Merelli, and N. Paoletti, "Multiple verification in computational modeling of bone pathologies," in *CompMod*, 2011, pp. 82–96.
[17] A. T. Bittig and A. M. Uhrmacher, "Spatial Modeling in Cell Biology at Multiple Levels," in *Proceedings of the 2010 Winter Simulation Conference*. IEEE, 2010, pp. 608–619.
[18] F. Ciocchetta and M. L. Guerriero, "Modelling Biological Compartments in Bio-PEPA," *Electronic Notes Theoretical Computer Science*, vol. 227, pp. 77–95, January 2009.
[19] A. Regev, E. M. Panina, W. Silverman, L. Cardelli, and E. Shapiro, "Bioambients: an abstraction for biological compartments," *Theoretical Computer Science*, vol. 325, no. 1, pp. 141 – 167, 2004.
[20] C. Priami and P. Quaglia, "Beta Binders for Biological Interactions," in *Computational Methods in Systems Biology*, ser. Lecture Notes in Computer Science, 2005, vol. 3082, pp. 20–33.
[21] L. Cardelli and P. Gardner, "Processes in Space," in *Programs, Proofs, Processes*, ser. Lecture Notes in Computer Science, 2010, vol. 6158, pp. 78–87.
[22] M. John, C. Lhoussaine, J. Niehren, and A. Uhrmacher, "The attributed π-calculus with priorities," *Transactions on Computational Systems Biology XII*, pp. 13–76, 2010.
[23] A. Stefanek, M. Vigliotti, and J. T. Bradley, "Spatial extension of stochastic π calculus," in *8th Workshop on Process Algebra and Stochastically Timed Activities*, August 2009, pp. 109–117.
[24] R. Milner, *A calculus of communicating systems*. Springer-Verlag, 1980, vol. 92.
[25] D. Epari, G. Duda, and M. Thompson, "Mechanobiology of bone healing and regeneration: in vivo models," *Proceedings of the Institution of Mechanical Engineers, Part H: Journal of Engineering in Medicine*, vol. 224, no. 12, pp. 1543–1553, 2010.
[26] S. Komarova, R. Smith, S. Dixon, S. Sims, and L. Wahl, "Mathematical model predicts a critical role for osteoclast autocrine regulation in the control of bone remodeling," *Bone*, vol. 33, no. 2, pp. 206–215, 2003.
[27] M. Ryser, N. Nigam, and S. Komarova, "Mathematical Modeling of Spatio-Temporal Dynamics of a Single Bone Multicellular Unit," *Journal of bone and mineral research*, vol. 24, no. 5, pp. 860–870, 2009.
[28] J. Hillston, *A compositional approach to performance modelling*. Cambridge Univ Pr, 1996, no. 12.
[29] M. North, T. Howe, N. Collier, and J. Vos, "A Declarative Model Assembly Infrastructure for Verification and Validation," in *Advancing Social Simulation: The First World Congress*. Springer Japan, 2007, pp. 129–140.
[30] X. Yang and Y. Young, *Handbook of Bioinspired Algorithms and Applications*. Chapman & Hall/CRC Computer and Information Science, 2005, ch. Cellular Automata, PDEs, and Pattern Formation.
[31] A. Edelstein and N. Agmon, "Brownian simulation of many-particle binding to a reversible receptor array," *Journal of Computational Physics*, vol. 132, no. 2, pp. 260–275, 1997.
[32] A. Looker, H. Wahner, W. Dunn, M. Calvo, T. Harris, S. Heyse, C. Johnston Jr, and R. Lindsay, "Updated data on proximal femur bone mineral levels of us adults," *Osteoporosis International*, vol. 8, no. 5, pp. 468–490, 1998.
[33] "T and Z scores," http://courses.washington.edu/bonephys/opbmdtz.html, Accessed: 10/11/2011.
[34] WHO Study Group on Assessment of Fracture Risk and its Application to Screening for Postmenopausal Osteoporosis, "Assessment of fracture risk and its application to screening for postmenopausal osteoporosis," Tech. Rep. 843, 1994.

Nicola Paoletti received the B.S. and the M.S. degree in Computer Science from the University of Camerino in 2008 and 2010, resp. Since 2011 he is a PhD student at the School of Information Sciences and Complex Systems at the University of Camerino. His research interests include formal methods for the specification and verification of complex systems; computational systems biology; modeling of multiscale systems.

Pietro Liò is a Senior Lecturer and a member of the Artificial Intelligence Division of The Computer Laboratory (the department of Computer Science), University of Cambridge. He has an interdisciplinary approach to research and teaching due to the fact that he holds a Ph.D. in Complex Systems and Non Linear Dynamics (School of Informatics, dept of Engineering of the University of Firenze, Italy) and a Ph.D. in (Theoretical) Genetics (University of Pavia, Italy). Main research interests: Modeling multiscale biological systems; emerging properties from microscale to macroscale in biology; Modeling methodologies, parameter estimation techniques, reverse engineering of biological circuits; Bioinspired technology. He has published more than 200 papers and organized several workshops and schools.

Emanuela Merelli is Associate Professor of Computer Science at University of Camerino, Italy, where she currently leads the Complex Systems Research Group. She is the coordinator of B.Sc and M.Sc Degree and Doctoral Program in Computer Science. Her research interests include Formal Methods for Modeling and Verification of Complex Systems, Formal Methods applied to Systems Biology and Biomedicine, Agent-based Modeling for Multi-level and Multi-scale systems.

Marco Viceconti is full Professor of Biomechanics at the Department of Mechanical Engineering at the University of Sheffield and Scientific Director of the Insigneo/Sheffield Research Institute. Before this he was the Technical Director of the Medical Technology Lab at the Rizzoli Orthopaedic Institute in Bologna, Italy. Prof. Viceconti has a Mechanical Engineering degree from the University of Bologna and a PhD from the University of Firenze. His main research interests are related to the development and validation of medical technology, especially that involving simulation, and primarily in relation to musculoskeletal diseases. He has published over 200 papers and serves as reviewer for many international funding agencies and peer-reviewed journals.